

E2Efold-3D: End-to-End Deep Learning Method for accurate *de novo* RNA 3D Structure Prediction

Tao Shen^{†1,2}, Zhihang Hu^{†1}, Zhangzhi Peng^{†2,4}, Jiayang Chen¹, Peng Xiong³, Liang Hong¹, Liangzhen Zheng^{2,3}, Yixuan Wang¹, Irwin King¹, Sheng Wang^{*3}, Siqu Sun^{*4,5}, and Yu Li^{*1,6}

¹Department of Computer Science and Engineering, The Chinese University of Hong Kong, Hong Kong SAR, China

²Shenzhen Institute of Advanced Technology, Chinese Academy of Sciences, Shenzhen, Guangdong, China

³Zelixer Biotech, Shanghai, China

⁴Research Institute of Intelligent Complex Systems, Fudan University, Shanghai, China

⁵Shanghai AI Laboratory, Shanghai, China

⁶The CUHK Shenzhen Research Institute, Hi-Tech Park, Nanshan, Shenzhen, China

Abstract

RNA structure determination and prediction can promote RNA-targeted drug development and engineerable synthetic elements design. But due to the intrinsic structural flexibility of RNAs, all the three mainstream structure determination methods (X-ray crystallography, NMR, and Cryo-EM) encounter challenges when resolving the RNA structures, which leads to the scarcity of the resolved RNA structures. Computational prediction approaches emerge as complementary to the experimental techniques. However, none of the *de novo* approaches is based on deep learning since too few structures are available. Instead, most of them apply the time-consuming sampling-based strategies, and their performance seems to hit the plateau. In this work, we develop the first end-to-end deep learning approach, E2Efold-3D, to accurately perform the *de novo* RNA structure prediction. Several novel components are proposed to overcome the data scarcity, such as a fully-differentiable end-to-end pipeline, secondary structure-assisted self-distillation, and parameter-efficient backbone formulation. Such designs are validated on the independent, non-overlapping RNA puzzle testing dataset and reach an average sub-4 Å root-mean-square deviation, demonstrating its superior performance compared to state-of-the-art approaches. Interestingly, it also achieves promising results when predicting RNA complex structures, a feat that none of the previous systems could accomplish. When E2Efold-3D is coupled with the experimental techniques, the RNA structure prediction field can be greatly advanced.

Introduction

The importance of RNAs has been increasingly appreciated in the past decades [1]. Considering the small number of encoded proteins in the human genome (only roughly 1.5% of the genome are encoded) and the essential roles of RNA molecules in cellular information transfer and gene expression regulation [2], RNA-centric studies, such as RNA-targeted drug development [3] and engineerable synthetic elements design [4], have been promoted dramatically in recent years. Approved by FDA in August 2020, Evrysdi (risdiplam), designed for spinal muscular atrophy treatment, became the first drug targeting RNA directly [5]. Therefore, high-resolution structural information of the related RNAs is crucial to further develop drugs, especially on the druggable pockets in their structures [1, 5].

*Corresponding Author. Email: liyu@cse.cuhk.edu.hk, siqisun@fudan.edu.cn, and realbigws@gmail.com.

Unfortunately, determining RNA 3D structures is not straightforward, and the RNAs with experimentally resolved tertiary remain scarce. As of May 2022, among roughly 190,000 structures deposited in the Protein Data Bank (PDB), only 0.9% are RNA-only structures, and 2.1% are RNA-containing complex structures [1, 6]. The relative dynamic structure and conformational heterogeneity of RNAs have posed challenges to the three mainstream molecular structure determination methods. The structural flexibility of RNAs, especially the large ones, makes it problematic to crystallize them and thus resolve their structures using X-ray crystallography. Although nuclear magnetic resonance (NMR) spectroscopy seems to be a suitable tool for RNA structure determination due to its compatibility with solution techniques, the chemical diversity of building blocks in RNA leads to the signal overlap in the NMR spectra [6], making the method limited to small RNAs. Cryogenic electron microscopy (Cryo-EM) is the new hope for the RNA structure field. However, despite the recent breakthrough of determining the *Tetrahymena* group I intron at 2.98 Å resolution [1], only two other RNA-only structures are resolved by Cryo-EM with resolutions better than 4.5 Å. The conformational heterogeneity poses severe challenges to particle clustering and computational modeling in the Cryo-EM data analysis.

Considering the challenges, researchers have developed a few computational methods to push the limit together with the experimental methods on the RNA 3D structure determination and prediction. The previous computational methods can be divided into two categories, template-based modeling approaches and *de novo* RNA folding simulation methods. ModeRNA [7] and RNAbuilder [8] are representative methods of the former category. However, due to the limited template library size, the performance of such methods has not met people’s expectations. Methods from the latter category, including FARFAR2 [9], 3dRNA [10], and SimRNA [11], are more popular. However, such methods usually require large-scale sampling, making them computational demanding. Furthermore, although the recent method based on deep learning, ARES [12], has made progress in structure scoring, how to pick the sampled structures remains an unsolved problem.

Despite the success of deep learning (DL) based approaches in the protein field [13] and RNA secondary structure prediction [14, 15], to the best of our knowledge, there is no such DL-based approach to perform *de novo* RNA 3D structure prediction. That is, directly output the final 3D structure using the sequence information alone. The main reason is the lack of data. After removing redundancy and low-resolution RNA structures, only around 1100 RNA structures have left. By large-scale sampling using FARFAR2 on RNA, it is possible to train a model for structure scoring using DL, like ARES [12]. Nonetheless, developing a deep learning model to predict the 3D structure directly with the above-limited data remains challenging.

We present the first end-to-end DL-based approach, E2Efold-3D, for *de novo* RNA 3D structure prediction. On the independent RNA puzzle dataset without overlapping with the training dataset, it can reach an average root-mean-square deviation (RMSD) of 3.9 Å. Several strategies are proposed to tackle the computational challenges in this problem. Firstly, E2Efold-3D is composed of a fully differentiable end-to-end deep learning model, which can directly output the coordinates of all atoms in a valid RNA 3D structure with minimal human interference. Such an end-to-end model can take the maximal usage of the existing data. Secondly, our method utilizes multi-aspect information of the RNA sequence to infer the 3D structure. In addition to the commonly used multiple sequence alignment (MSA), containing the evolutionary information, we also take advantage of the information from a newly proposed RNA foundation model (RNA-FM) [15], which was trained on 23 million non-redundant RNA sequences in a self-supervised manner. The informative representation of the RNA sequence extracted from the large-scale database also alleviates the data scarcity problem. Thirdly, in addition to training against the 3D structure, we also introduce secondary structure information into the loss function. As the secondary structure data are much larger, and we have achieved satisfactory performance on the task [15], this idea further significantly augments the potential data we can use. Meanwhile, by simultaneously optimizing the secondary structure and 3D structure, E2Efold-3D is forced to try to capture the RNA folding process instead of only memorizing the training data, which may lead to overfitting. Finally, inspired by AlphaFold [13], we also developed a novel procedure to perform self-distillation. We use the sec-

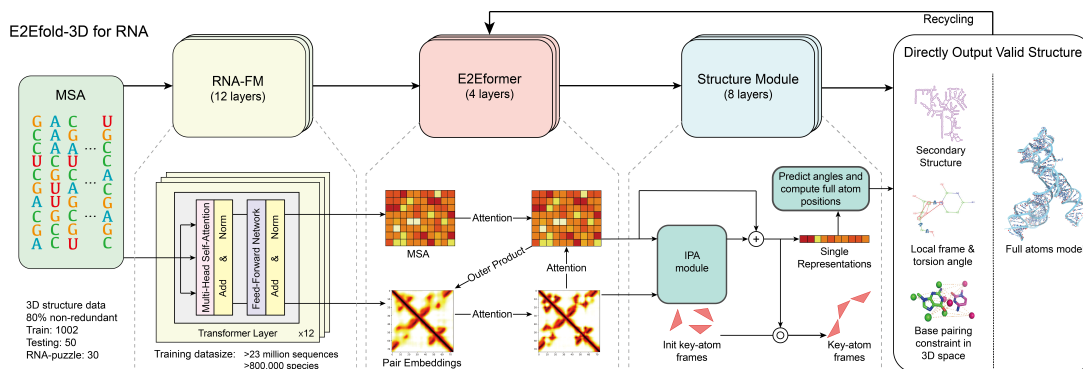


Figure 1: A overview of E2Efold-3D. E2Efold-3D is a fully differentiable end-to-end approach to perform *de novo* RNA 3D structure prediction using their sequence information. To initialize the sequence presentation of the query sequence and pair embeddings, the MSA of the query sequence will be passed through a pre-trained RNA foundation model. Afterward, these features will proceed through the E2Eformer and structure model to get the 3D structure. The loss function in E2Efold-3D contains additional structural constraints, allowing it to generate valid 3D structures directly. As a result, E2Efold-3D can perform well on the non-overlapping independent RNA-Puzzles testing dataset, with RMSDs of less than 4Å. In addition, the average inference time of E2Efold-3D is 0.14 seconds, which is significantly faster than FARFAR2’s 5086 seconds for one structure.

ondary structure label to explicitly select the confidently predicted structures and use them to augment the training dataset. With the above strategies, we can reach a sub-4 Å resolution RNA 3D structure prediction on the RNA puzzle dataset, which outperforms the state-of-the-art method, FARFAR2, by a large margin. Even sampling more than 48K structures on some targets, FARFAR2 can only achieve the average RMSD score of 7.3 Å on the standard dataset. Further experiments show that with minimal adjustment to the model architecture and only changing the loss function, we can also reach promising results on the RNA complex structure prediction. E2Efold-3D is a pioneering deep learning method in this direction, which would hopefully lead to the advancement of resolving the RNA structure.

Results

Overview of E2Efold-3D E2Efold-3D is a fully differentiable end-to-end method to perform *de novo* RNA three-dimensional structure prediction from sequences alone. Its overview is illustrated in Figure 1. To enrich the structural information from a huge amount of unlabeled data, an RNA foundation model [15] is first initialized as sequence representations. The extracted sequence features and the corresponding MSA are then fed through a 4-layer E2Eformer module to learn the sequence representations and interactions between different nucleotides. E2Eformer embeddings are subsequently sent to an 8-layer structure module and used to generate the final RNA 3D structures.

In contrast to previous approaches, the entire model is fully differentiable so that we can optimize directly against full atom coordinates. We then add several additional constraints to the structure output to ensure the final output is valid without clashing structures, such as secondary structure and base pairing constraints. In addition, the secondary structures are used to select high-confidence predicted structures for use as additional training data in the large-scale deep learning-based model since the ground truth data set is limited to only around 1000 structures. Finally, we employ the recycling technique similar to AlphaFold to enhance prediction accuracy. In the following sections, we provide a detailed analysis of the data and the effectiveness of the proposed method.

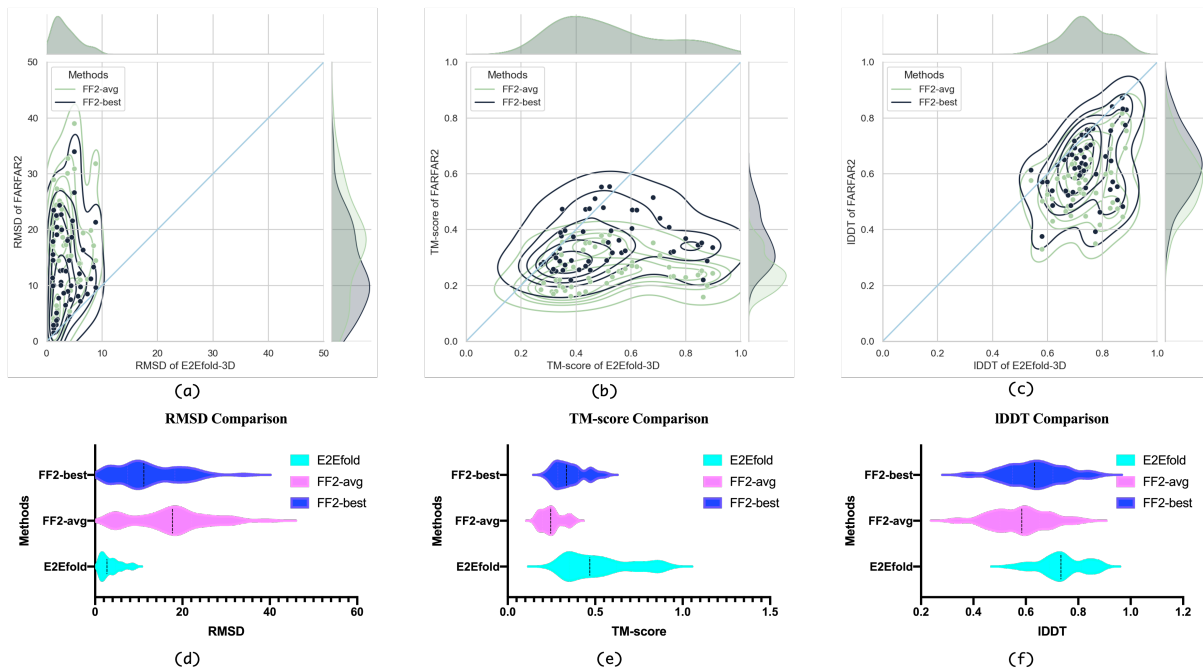


Figure 2: Performance analysis of the E2Efold-3D on the test set with 50 structures. (a-c) A head-to-head comparison between E2Efold-3D and FARFAR2 (FF2), using RMSD, TM-score, and IDDT. The x-axis shows the performance of the E2Efold-3D, while the y-axis shows the performance of FARFAR2. Each point represents one RNA. We compare our method with both the best structure (FF2-min) and the average structure (FF2-avg) generated by FARFAR2. (d-f) Violin plots of different methods’ performance on the testing dataset, with respect to RMSD, TM-score, and IDDT.

Standardize the training and testing datasets The main obstacle to developing RNA 3D structure prediction methods is the lack of data. We have assembled a comprehensive dataset that includes data from Protein Data Bank and BGSU RNA Representative Sets with experimentally determined structures, and 4012 RNAs with complex folds have been curated. To eliminate redundancies in the dataset, we use a cutoff of 80% sequence identity and remove RNAs that exceed the range of 20-512 nucleotides. Eventually, we construct a training dataset with 1002 structures, a testing dataset with 50 structures, and an independent testing dataset with 30 challenging RNA targets from the community-wide RNA-Puzzles experiments. The raw RNA-Puzzle dataset is publicly available at Github. As the training dataset size is very small, we attempt to augment the data. To begin with, we re-integrating the sequence clusters which have been redundancy-filtered back into the training data. Notice that there is no information leakage between the testing datasets and the augmented training datasets since the 80 percent sequence identity cutoff still applies. In addition, we also include the RNA chains from complexes as separate training data points. For the final training set, there are 2728 single-chain RNAs and 677 complexes, resulting in a total of 3833 RNA chains.

Accurate predictions on independent non-redundant test set Our first step towards analyzing our performance was to compare our E2Efold-3D with FARFAR2 [16], one of the most popular RNA folding models that achieve state-of-the-art levels of performance. The results are presented in Table 1 in terms of the average and median RMSD, IDDT, and TM-score against experimental structures. Here, RMSD represents a measure of the average distance between atoms of superimposed RNA; TM-score is a metric for assessing structural similarity that is based upon a value in the range [0, 1]. A score of one indicates a structural match, and a score above 0.5 indicates that two RNA molecules share the same global fold; Local Distance Difference Test (IDDT) scores quantify the degree to which interatomic distances in

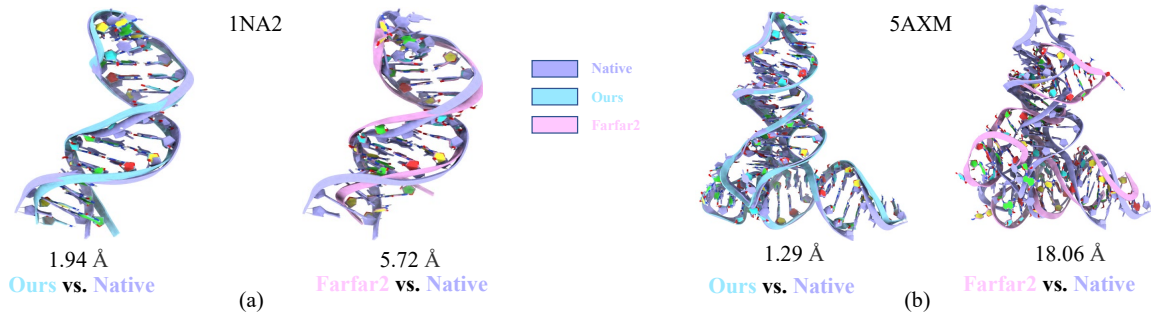


Figure 3: Visualization of structures resulting from different models. We choose two representative RNA structures from the testing dataset with 50 RNAs. 1NA2 is a telomerase RNA p2b hairpin, and 5AXMP is a tRNA. Structures generated by our method and FARFAR2 are aligned to native structures, which are visualized using ChimeraX. It has been demonstrated that the structures predicted by E2Efold-3D are very well matched with the native structures.

Table 1: Quantitative comparison between E2Efold-3D and FARFAR2 on the test set with 50 curated RNAs. The results are presented as an average score for each method. “FARFAR2-best” means we calculate the evaluation metric using the best structure generated by FARFAR2. “FARFAR2-avg” refers to the average score of all the sampled structures from FARFAR2.

Method	RMSD (Å)	TM-score	IDDT
FARFAR2-best	12.555	0.354	0.633
FARFAR2-avg	17.165	0.249	0.573
E2Efold-3D	3.486	0.518	0.739

the reference structure are replicated in the second structure. As presented, the performance of our model is significantly better than that of FARFAR2 across all metrics. Due to the large number of decoys generated by FARFAR2, and the fact that different algorithms for ranking the decoys will produce different results, we have computed the performance for FARFAR2-avg and FARFAR2-best to serve as the lower and upper bound, respectively. FARFAR2-avg represents the average result of all trials, and FARFAR2-best represents the performance associated with a perfect ranking algorithm that selects the very best decoy irrespective of whether the selection is challenging. Thus, FARFAR2-best represents the theoretical upper bound of the algorithm.

Table 1 summarizes the statistical results of E2Efold-3D on our independent non-redundant test set. Across 50 samples, E2Efold-3D achieved an average TM-score of 0.5175, which outperforms around twice better than results attained by FARFAR2-avg (0.2492) and 180% higher than even FARFAR2-best. Note that the average of TM-score is above 0.5, suggesting that we produce matching folds across most samples. In examining IDDT values, significant differences were observed, with 0.7385 against 0.5726/0.633 for the comparison with E2Efold-3D and FARFAR2-avg/best. Moreover, the average RMSD of E2Efold-3D was 3.4864 Å compared to 17.1645 Å/12.555 Å for FARFAR2-avg/best. The differences were again highly significant since we are almost 400% better. Our findings show a good match between the predicted and native structures at the atomic level. Taking into account even the minimum RMSD values, FARFAR2 produced an average minimum RMSD of 12.6780 Å, which is still significantly worse than our results. In terms of the maximum TM-score, FARFAR2 reaches a value of 0.3514, which is still around 0.15 below the proposed approach.

Figure 2 summarizes our performance via different aspects. As shown in Figure 2(a)-(c), we present head-to-head RMSD, TM-score and IDDT comparisons of E2Efold-3D with FARFAR2. Within each scatterplot, each point represents a specific sample within our test set. The green and black colors refer to average and best predictions, respectively. The y-axis stands for results for FARFAR2 while

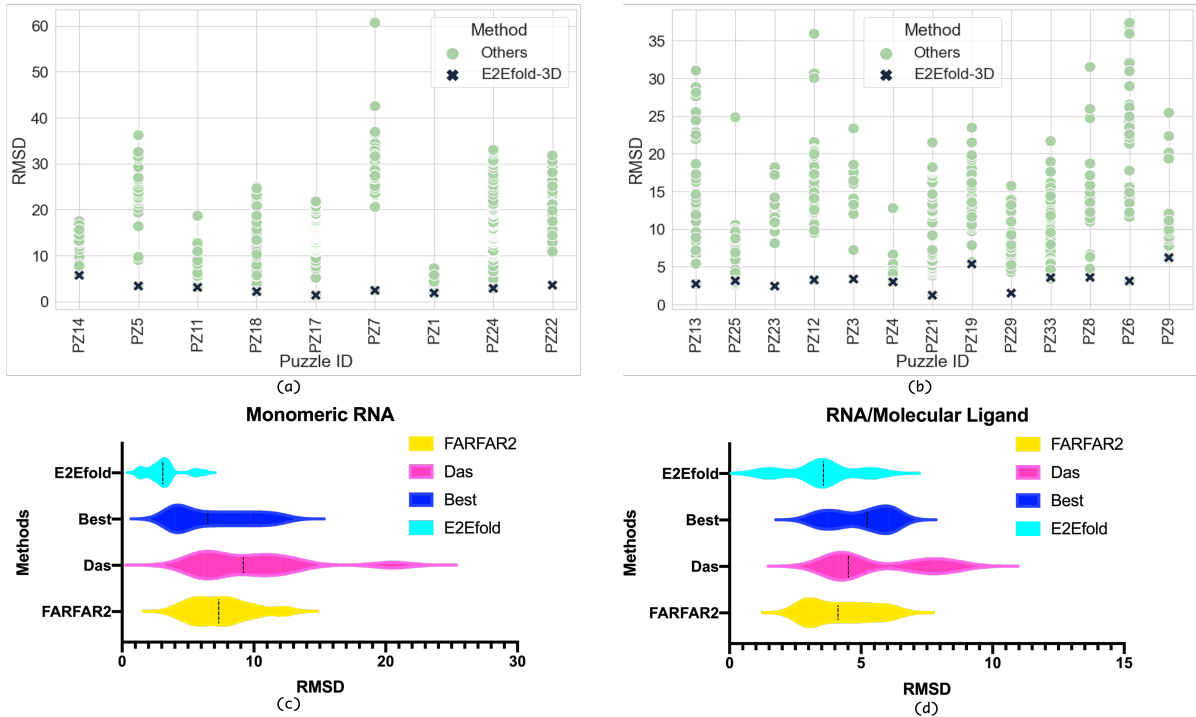


Figure 4: Comparison of performance of different methods on the RNA-Puzzles structures. (a,b) Comparison of detailed RMSD scores between RNA 3D models. 'Others' refers to the results of various methods obtained from the RNA-Puzzle community. The x-axis shows the ID of the tested RNA. Each point represents a structure predicted using a particular method. Figure (a) shows the performance of the single-chain RNA, and Figure (b) shows the performance of the RNA complexes. (c,d) Violin plots of the performance of different methods on RNA puzzles.

the x-axis for E2Efold-3D, and the dots below the diagonal line suggest our measurement outperforms FARFAR2, vice versa. (a) demonstrates our perfect predictions where all data points lay below the diagonal. Furthermore, some outliers exist in (b) or (c), in which those RNAs are of long length and have a shallower MSA, making the predictions random, thus making it difficult to gain an edge over FARFAR2. In addition, (d) to (f) present each model's violin plot of the result distribution. Evidently, E2Efold-3D's reached the best average score across every metric while remaining lowest variance among RMSD and IDDT. A higher variance is observed in the TM-score, which is consistent with (b) that a few outliers reduced the performance of the TM-score.

Case studies on two RNA samples within our test set is presented in Figure 3. Figure 3(a) 1NA2 represents the solution structure of the p2b hairpin from human telomerase RNA, comprised of 30 nucleotides. This means an RMSD of 1.94\AA , which is approximately three times better than FARFAR2. It is noteworthy that the TM-score of our prediction is similar to FARFAR2, and this example represents one of the outliers above the diagonal in Figure 2(b), where the mismatch occurs in the tail of 1NA2. Figure 3(b) is a structure of Thg1-like protein (TLP) with tRNA (Phe), which is relatively long with 251 nucleotides. We have obtained surprisingly accurate results, with an RMSD of 1.29\AA compared to 18.06\AA of FARFAR2. The length of the nucleotide chain does not adversely affect our performance in this case. And we achieve a significantly higher TM-score (0.8445) than FARFAR2 (0.2345), in contrast to (a). Thus, the above example demonstrates the efficacy of the proposed approach.

Best results across two RNA-Puzzle categories. In addition to our curated test set, we further examine our model on RNA-Puzzles. A total of 22 samples of RNAs were selected from the community-wide as RNA-Puzzles benchmark, most of which have no structural information or sequence homology, thus

Table 2: Quantitative comparison between E2Efold-3D and FARFAR2 on the RNA-Puzzles structures. In this study, we demonstrate the performance of various methods both for the single RNA chain and for the RNA-Ligand complex. The average scores for each method are presented. As for the approaches relating to FARFAR2, we utilized the results in their original paper. Please note that a large-scale sampling is performed for each structure for FARFAR2. On average, FARFAR2 generates 23,988 models for each RNA.

Method	Monomeric		RNA/Molecular Ligand	
	RMSD (Å)	TM-score	RMSD (Å)	TM-score
Best Model(All Submission)	8.512	0.435	6.691	0.440
Best Model(Das Model)	9.249	0.368	7.024	0.428
FARFAR2(top 1%)	6.548	-	5.034	0.382
E2Efold-3D	2.938	0.649	3.272	0.555

making identification of the instances challenging. Prior best results from the RNA-Puzzle server can be found at the official server ¹. Notice that the results involve two categories: the Server group and the Human group. The server groups work on a computational basis, and 48 hours are assigned to conduct RNA predictions. In contrast, human groups are composed of human experts who employ expert knowledge to infer structure. As a result, Human groups are given 3-6 weeks to solve a structure model and typically perform better than their Server counterparts. In conducting our evaluations, we separated RNA-Puzzle into two types: Monomeric RNA and RNA/Molecular Ligand to study the performance of these two RNA types.

Monomeric RNA is the simplest type of RNA, consisting only of a single chain within its structure. RNA-Puzzle contains 9 monomeric RNAs and Table summarizes our performance. The analysis is conducted with two promising methods: FARFAR2, Das, and another statistic from selecting the best predictions for each RNA sample ². We concluded that the proposed approach achieved the best performance for all metrics, with an average RMSD of 2.938, about twice as good as the next-best model (FARFAR2 top 1%: 6.548). In terms of TM-score we also achieved an average of 0.649, almost 80 percent higher than that of the top-performers (0.435). The difference is even more significant when considering the results of the Das group. Additionally, our model predicts structures that is primarily consistent with the ground truth if 0.5 is regarded as the TM-score cutoff.

Figure 4 visualizes our predictions along with other results on every RNA sample obtained from the RNA-puzzle server. (a) & (c) refers to monomeric RNA, and each dot within (a) corresponds to a specific result for each method. Clearly, our predictions have the lowest RMSD across all samples. It is noteworthy that these ‘grey’ dots involved human groups and handcrafted results, suggesting that we can outperform human experts to some extent. The margin is relatively large at 27, which belongs to T-box riboswitch puzzles, indicating that we are capable of making outstanding predictions of this type.

RNA/Molecular Ligand is a complex of a RNA/Molecular bound with a ligand interacting with each other or with various other molecules. Theoretically, it involves interactions with other molecules and is more difficult to predict. In RNA-puzzle, we identified 13 RNA/molecular/ligand complexes, possibly insufficient to differentiate between monomeric and polymeric RNAs.

The same applies to Table 2, and we still achieved the best score across RMSD and TM-score, with an average RMSD of 3.272 and TM-score of 0.555, respectively. It is of interest to note that the margin is still large, 1.8 Å for RMSD and 0.120 for TM-score, but smaller than Monomeric RNA, which is likely a result of the small number of samples of both categories, and the average length is short (around 70 nt). Using TM-score=0.5 as a cutoff, our model predicts nearly consistent structure with the ground

¹<http://www.rnapuzzles.org/>

²TM-score for FARFAR2 is missing.

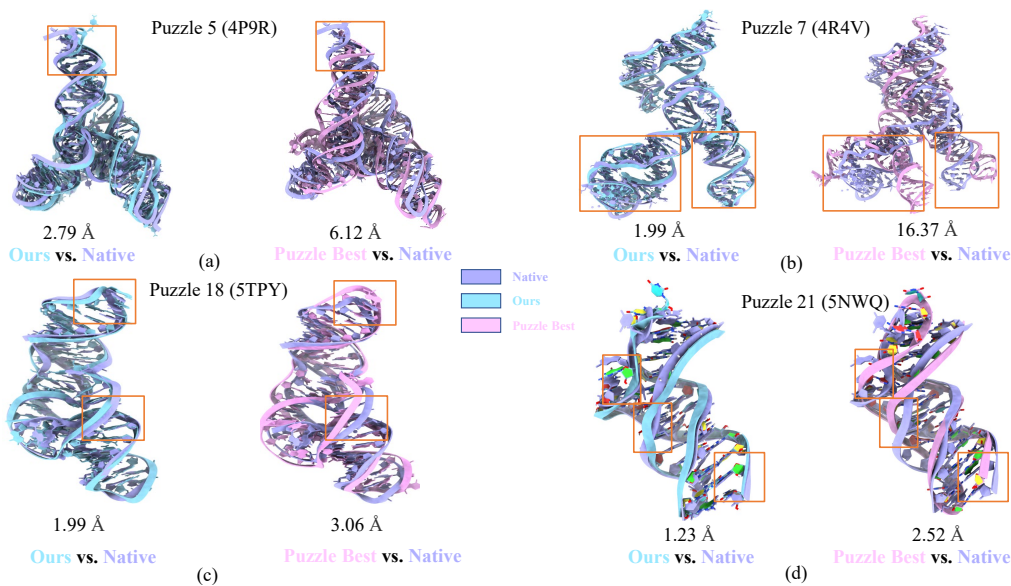


Figure 5: Visualization of predicted and native RNA structures of four representative cases from RNA-Puzzles. Left: ours VS native. Right: best structure submitted by RNA-Puzzle community VS Native. Orange boxes highlight the structural differences. (a) 4P9R is a lariat capping ribozyme. (b) 4R4V is the Varkud satellite ribozyme. (c) 5TPY is an exonuclease resistant RNA from Zika virus. (d) 5NWQ shows the structure of the thermobifida fusca guanidine III riboswitch.

truth (fails on RNA Puzzle 19).

Figure 4 again illustrates our predictions alongside other results for every RNA sample obtained from the RNA-puzzle server. In this example, (b) & (d) are the RNA/Molecular/Ligand Complexes and each dot corresponds to the result of each method. Despite our consistently low RMSD across all samples, this difference is insignificant in RNA Puzzle 28/8/19. This group of three RNAs has relatively fewer MSA depths, which probably contributes to their defects.

Case studies for four representative cases of RNA-Puzzle are represented in Figure 4, in which our E2Efold-3D achieves near-native accuracy with an average RMSD value of only 2.00 Å. In contrast, the state-of-the-art methods achieve an average RMSD value of 7.02 Å. Figure 5 (a) illustrates the structure of Puzzle 5, which is a 189-nucleotides lariat-capping (LC) ribozyme (PDB ID: 4P9R) [17]. As indicated by the orange box, the best baseline fails to predict the fold at the top, while our model produces a near-native fold. Figure 5 (b) shows the structure model of Puzzle 7, which is a 186-nucleotides intertwined dimer formed by an exchange of substrate helices (PDB ID: 4R4V) [18]. As shown in the orange boxes to the right, even the best model from RNA-Puzzle community results in an incorrect fold, which has an RMSD of 16.37 Å. Our model, on the other hand, accurately predicts the structure with a RMSD of 1.99Å. Figure 5 (c) presents the 3D model of Puzzle 18, which is a 71-nucleotides RNA motif with a multi-pseudoknot structure (PDB ID: 5TPY) [19]. A closer inspection of the puzzle-best structure reveals that its prediction has gaps in several areas, as described by the boxes. We have found that these phenomena are largely mitigated by our model, where we predict with almost native accuracy. Figure 5 (d) shows the structure model of Puzzle 21, a ykkC guanidine III riboswitch from *Thermobifida fusca* (PDB ID: 5NWQ) [19] with 41 nucleotides. We observe similar phenomena as in Figure 5 (c): the proposed model accurately predicts many areas that are improperly predicted by baselines.

Automated *de novo* RNA complex prediction. RNAs can link to each other and form complexes having catalytic functions. A well-known example is the ribosome structure and ribosomal proteins. RNA complexes are formed by canonical interactions (A-U, G-C) and the Wobble base pair (G-U) between several strands of RNA as well as by noncanonical interactions. In spite of preserving complicated

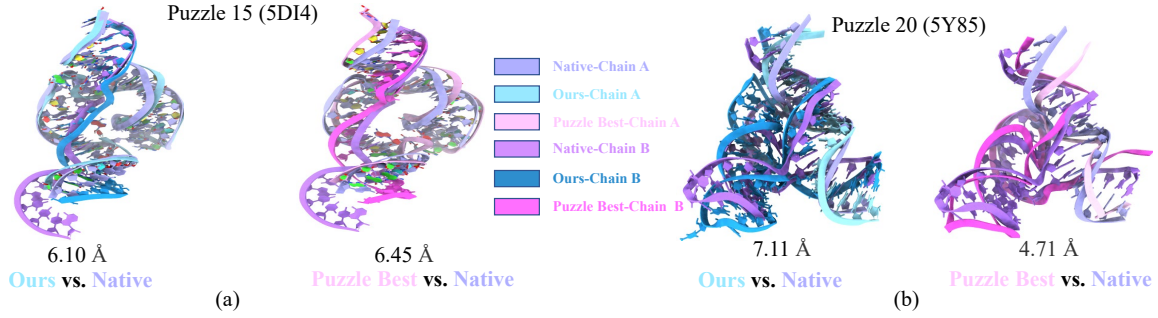


Figure 6: Visualization of predicted and native RNA structures from two representative RNA complexes from RNA-Puzzles. The predictions derived from E2Efold-3D are aligned with native structures and then visualized. Additionally, we illustrate the alignment of the previously best-predicted structure from the community with the native structure. (a) 5DI4 is a hammerhead ribozyme with two chains. (b) 5Y85 shows the structure of a twister-sister ribozyme with two chains.

interactions and multiple chains, predicting RNA complexes remains a substantial challenge. Within RNA-Puzzle, seven RNA complexes are proposed, and most submitted results relate to RMSDs over 10 Å, indicating a significant discrepancy between predictions and ground truth. Currently, the majority of RNA complex prediction methods rely on human knowledge, and there is no automated de novo pipeline available. We present here two examples of predicted RNA complexes using our end-to-end de novo pipeline.

RNA Puzzle 15 is the hammerhead ribozyme (PDB ID: 5DI4) with two chains (Chain A: 48 bases, Chain B: 20 bases). It is one of the earliest discovered nucleolytic ribozymes, which are ubiquitous across the tree of life and have potential therapeutic applications. In its 3D structure, the two chains form three helices, which are linked by sequences with conserved motifs “CUGA” and “GAAA”. In Figure 6(b), we present a comparison between our prediction and the native structure, as well as an alignment between the Puzzle Best structure and the native structure. The model achieves satisfactory performance on this complex, with a lower RMSD (6.10 Å) than the Puzzle Best (6.45 Å). In addition, most conformation of Chain A is predicted correctly. Regarding the interaction between the two chains, one of the two interaction helices has been recovered. Note, however, that the deviation of the last helix is quite significant due to the imperfect prediction of the complex folding. While the E2Efold-3D is already superior to the Puzzle Best in this particular case, it is necessary to improve the prediction of interactions to facilitate 3D structure predictions.

RNA Puzzle 20 is a twister sister ribozyme (PDB ID: 5Y87) with the self-cleaving property. It comprises two chains (Chain A: 18 bases, Chain B: 50 bases), which are co-axial stacked helical sections. The ribozyme has two crystal structures in the PDB database: three-way junctional or four-way junctional ribozymes. In this example, we compare the predictions of our method with those of four-way junctional twister sister ribozymes, as shown in Figure 6(b). Overall, E2Efold-3D does not perform impressively on the complex with the RMSD=7.11 Å, worse than the Puzzle Best’s 4.71 Å. It appears that the co-axial helical sections and the interactions between the two chains are approximately predicted. However, the hairpin 3D structure of chain B is not correctly recovered. Due to the pseudoknots in the secondary structure, the overall 3D structure is quite complex. It may be possible to improve performance in such situations if a more elaborate prediction of pseudoknots is made.

Strong correlation between local-distance difference test. Despite the improvements in our accuracy over previous measurements, we provide another assessment of our performance similar to AlphaFold2 [13]. Figure 7 shows the relationship between the predicted local distance difference test (pLDDT) and the local distance difference test (lDDT). Each dot in the scatterplot (a) stands for an RNA sample. In this case, all samples from the test set and RNA puzzle are included. Since we conducted

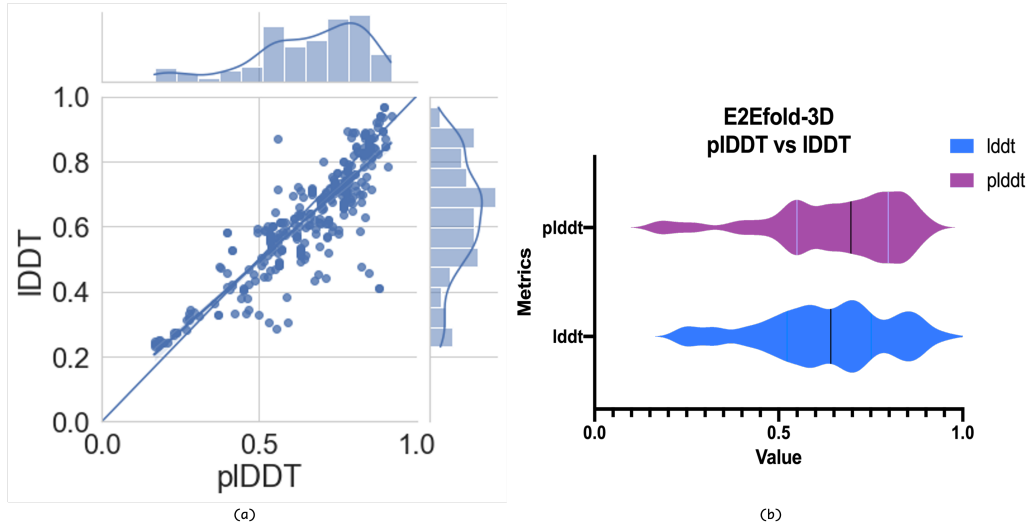


Figure 7: Visualization of our predicted local-distance difference test against local-distance difference test. Scatterplot (a) presents the comparison of each sample, suggesting a highly correlated result. Violin plot (b) illustrates these two distributions.

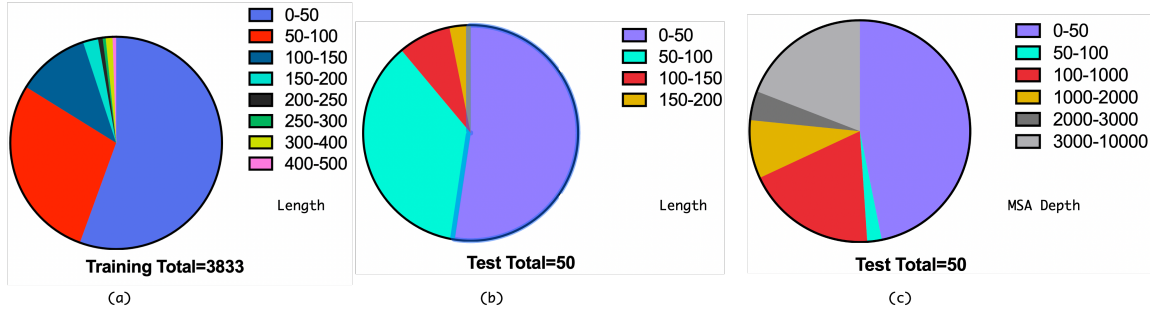


Figure 8: Distribution of sequence length and MSA depth in training and testing set. (a),(b) and (c) indicate that most of the data are short sequences with few homologs.

multiple trials for each RNA, there actually exist more than 350 dots within this figure. Different MSA depth, recycling periods, and even sequence masking are considered. Therefore, an average of seven trials per sample are conducted. The fact that each dot lies near the diagonal line suggests that our pIDDT are highly correlated with IDDT, and the Pearson correlation is calculated at 0.8816. The violin plot (b) indicates that pIDDT per sample is closely related to IDDT, both in terms of their form as well as position near the x-axis. Consequently, these results confirm our capability to predict RNA 3D structure accurately.

Sequence length and homolog depth affect prediction accuracy. We observed some huge variances between the different RNA samples when conducting predictions on our test set. Upon further inspection, interesting phenomena suggest that RNA length and MSA depth may influence the accuracy of the prediction. Therefore, we first examine the distribution of sequence lengths and MSA depths among our training and test set illustrated in Figure 8. As indicated by (a) and (b), most sequences in both sets have a length below 100, while sequences above 200 are extremely rare. Interestingly, (c) reveals that approximately half of our sequences receive very few homologs (<50) while the other half receive over 100 homologs.

Furthermore, Figure 9 shows ablation studies of these two factors. Figure 9(a) reveals the relationship between TM-scores and sequence lengths. We therefore observe that both too long and too short

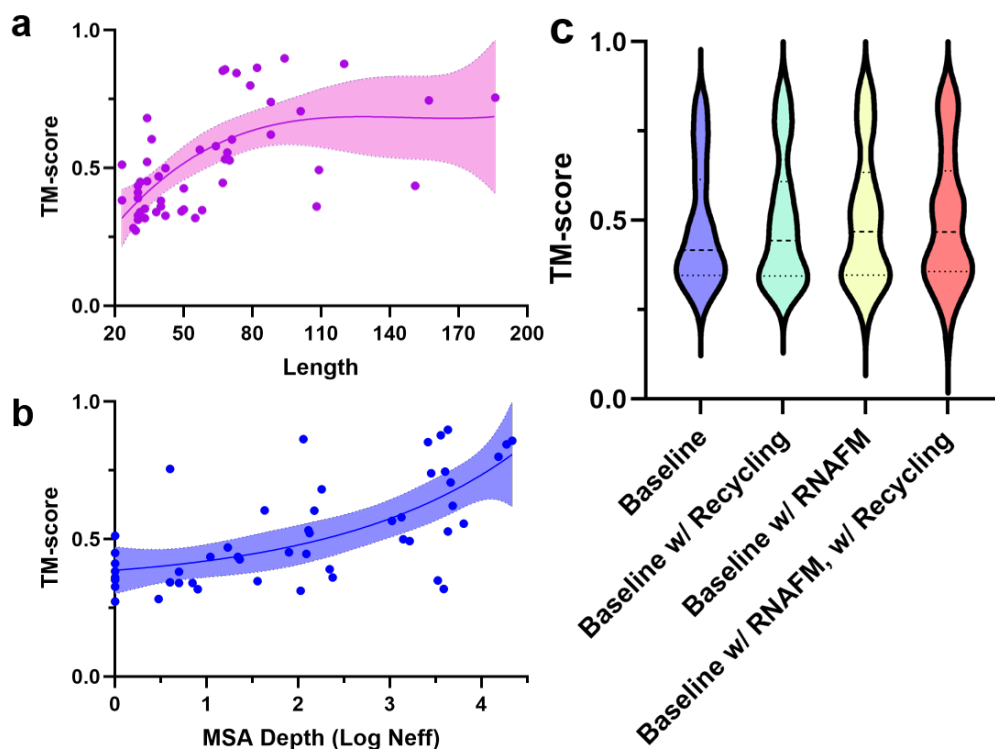


Figure 9: Detailed performance analysis and ablation study. (a) TM-score VS RNA sequence length. Each point represents a particular test RNA. The performance of E2Efold-3D is not compromised by the long RNAs, despite the fact that the data is unbalanced by the length of the RNAs. (b) TM-score VS the MSA depth of the query RNA sequence. E2Efold-3D performs better when there are more sequences in the MSA. (c) An ablation study on RNA-FM and recycling in the method. Both of these factors contribute to improvements in the performance of E2Efold-3D.

sequences can negatively impact our performance, while the best predicting interval lies in [60,110]. Figure 9(b) examines the model performance with respect to the quality of the MSA depths. The y-axis indicates the TM-score of E2Efold-3D, and the x-axis indicates the logarithm of the MSA Neff value. Noted that several RNAs within our test set lack sequence homologs, and that the average TM-score could be slightly lower by 0.2 than other MSA Neff values. A defect of this type would generally be acceptable since most RNAs are located within an adequate MSA depth. Moreover, a TM-score of 0.5 indicates a close match between the model and reality, and thus our model is robust against very challenging targets producing an average TM-score of 0.43.

RNA-FM features and recycle module boost the model’s performance. We further perform ablation studies to evaluate the contribution of different components within our method. As we discussed, we use a pre-trained RNA foundation model to extract information from the 23 million RNA sequence database, which could implicitly augment the data. Moreover, we make use of the recycling concept to augment the training data explicitly by utilizing the high-confidence prediction structures as additional training data. We therefore evaluate the performance change of both components one at a time after eliminating them from our method. As shown in Table 3, both components contribute to the improvement in performance. It is interesting to note that the RNA-FM features contribute more to TM-score improvement, whereas the recycling module plays a greater role in RMSD. It could be that RNA-FM is a global feature, while recycling would result in local refinement. As they are orthogonal to each other, integrating both into E2Efold-3D provides the greatest performance gain. However, we must acknowl-

Table 3: **Ablation study on different components of our method.** We assess the contribution of RNA-FM embeddings and the recycling process since the former can implicitly augment the data, while the latter can implicitly augment the data. They are orthogonal to each other and the two can contribute to improving performance. Experiments were conducted on 50 test structures in each method.

Model	TM score	RMSD(Å)
E2Efold-3D	0.481	4.703
E2Efold-3D w/ Recycling	0.498	4.614
E2Efold-3D w/ RNA-FM	0.503	4.748
E2Efold-3D w/ RNA-FM, w/ Recycling	0.504	4.525

edge that such two approaches don’t offer much improvement in the worst cases. As shown in Figure 9(c), the bottom of the performance violin plots does not improve even when both techniques are added.

Swift predictions within a second. In the context of applying computational models to large-scale real-world scenarios, speed is a crucial consideration. One benefit of E2Efold-3D is that it allows highly accurate RNA prediction in just a few seconds. E2Efold-3D has an average inference time of 0.12s, while FARFAR2 has an average inference time of 4,777s, or almost 40,000 times slower. The latter is unacceptable for a dataset with a million scale. Table4 lists some examples of running time on RNA Puzzle. Clearly, the entire prediction process for E2Efold-3D without refinement does not take more than a second. In the case of multiple FARFAR2 models, the average running time is 92,337,793 seconds, approximately 769,481,608 times slower than ours. Please note that the refinement process, in this case, is unnecessary because it involves additional optimization (500 iterations) with little effect on accuracy.

Discussion and Conclusion

In this work, we develop the first end-to-end deep learning method, E2Efold-3D, to predict the RNA 3D structure. By using a fully-differentiable model and new strategies to augment the training data, either implicitly or explicitly, we are able to achieve a sub-4 Å resolution on the prediction of the non-overlapping and non-redundant RNA puzzle structures, which far outperforms previous computational approaches. In addition, because our method does not require a time-consuming and computationally intensive sampling process, it is convenient and efficient.

Even though our method performs exceptionally well on the existing dataset, we must admit that it is imperfect and cannot solve the problem of predicting the RNA 3D structure completely. Due to the limited amount of training data, namely the lack of large RNA structures and complex RNA structures, the performance of our method on such RNAs is less accurate, which could be improved in the future. Additionally, structural flexibility and conformation heterogeneity are intrinsic properties of RNAs. These characteristics are currently beyond the capability of current methods.

As we have discussed,, the process of determining the structure of RNA is even more complex than that of predicting the structure of proteins [1]. It is essential that computational researchers collaborate with experimental researchers in order to advance the field [6]. For instance, the predictions derived from our method may provide an initial model for the analysis of cryo-EM data, which may significantly improve the resolution of the resolved structure [20]. Additionally, we expect to further improve our method’s performance with additional accumulated data in the future, such as large RNA structures.

Table 4: **The running time of RNA 3D structure prediction methods on RNA-Puzzles.** E2Efold-3D is capable of producing valid structures directly. Because it is a deep learning method that eliminates the time-consuming sampling process, it can predict a structure in less than a second. By comparison, it takes FARFAR2 5086 seconds to sample a structure. Considering FARFAR2 samples multiple structures, the time gained by E2Efold-3D is even more substantial.

Puzzle	ID	Length	FARFAR2	FARFAR2-Runtime (s)		E2Efold-3D-Runtime (s)	
			Num Model	Single model	All models	w/o Refine	w/ Refine ^a
3	3OXE	84	33442	4200	1.40E+08	0.10	249.42
4	3V7E	126	5768	10416	6.01E+07	0.17	402.59
5	4P9R	188	24903	10800	2.69E+08	0.31	786.15
6	4GXY	158	28859	8712	2.51E+08	0.27	608.19
7	4R4V	185	7963	13080	1.04E+08	0.25	741.13
8	4L81	96	33086	3270	1.08E+08	0.16	262.07
9	5KPY	71	18660	2256	4.21E+07	0.10	153.54
11	5LYU	57	41952	1410	5.92E+07	0.10	98.99
12	4QLM	117	35506	8298	2.95E+08	0.13	304.84
13	4XW7	60	20297	2118	4.30E+07	0.10	119.85
14b	5DDP	61	24531	2640	6.48E+07	0.11	114.82
14f	5DDO	61	15112	1932	2.92E+07	0.09	113.56
18	5TPY	71	17091	3636	6.21E+07	0.09	173.43
19	5T5A	62	4499	2166	9.74E+06	0.10	121.68
21	5NWQ	41	48146	1350	6.50E+07	0.10	74.27
Avg	-	96	23988	5086	1.07E+08	0.14	288.30

^a Refinement refers to an additional optimization (500 iterations) following our E2E model prediction in order to obtain more reasonable visualization. Actually, it almost has no effect on our model’s performance.

Methods

As we discussed in the result section, our deep learning model E2Efold-3D significantly improves the accuracy of RNA 3D folding by taking RNA sequence as the only input. Following this, we will proceed to describe the details of the pipeline, which consists of three main components: the feature extraction module, the structure prediction module, and the structure refinement module, as illustrated in Figure 1.

Feature extraction by RNA-FM and E2Eformer. Input features are divided into two folds to capture MSA co-evolution information and the structural information encoded in an enormous amount of unlabeled data. Using the query RNA sequence, the MSA and pairwise residue features are derived from the Infernal and rMSA protocol by searching from Rfam [21] and RNACentral [22]. Infernal is a covariance-based method for finding homologs with more secondary structure conservation than primary sequences, while rMSA uses a hierarchical approach. The searched MSA is encoded into a one-hot vector and mapped into embeddings using a linear layer with learnable positional encodings. Alternatively, RNA-FM, a pre-trained language model based on 23 million RNA sequences, has been demonstrated to perform well on a wide range of structure prediction tasks [15]. As a result, it enriches the structural information gained from unlabeled sequences, greatly alleviating the data scarcity problem. The two sets of features are finally combined and fed into the proposed E2Eformer module.

As with the Evoformer introduced in AlphaFold [23], E2Eformer consists of a series of gated attention layers that are applied to learn evolutionary information and update the MSA representation simultaneously. By mapping row-wise features to queries, keys, and values with linear layers, the row-

wise gated attention layer computes an affinity matrix by using the dot product between queries and keys, then it feeds this to the softmax function to create the attention matrix. After the attention matrix is applied to the values, the gating term is scaled by the dot product. A self-attention module is also applied on the column-wise gated attention layer. After the resultant MSA representation is constructed, a transition layer composed of two linear layers expands the embedding dimension by a factor of four and maps it back to the original dimension. Lastly, the E2Eformer is stacked with four blocks to refine the MSA and pair representation. Afterward, the output sequence and pair representation are fed into the structure module, which we will discuss next.

A novel structure prediction module. The structure module in E2Efold-3D aims to predict the 3D structure of an RNA given the extracted sequence and pair representation from E2Eformer. In AlphaFold [23], the structure module directly predicts the rotation and translation matrix of the main frames since they are the significant factors determining protein folding. And yet, the RNA folding is primarily driven by the base-pairing at nucleobase. In our experiments, directly predicting the base frame ($C1'$, $N1/N9$, $C2/C4$) defined over the nucleobase will result in a convergence problem due to their irregular structural patterns. To resolve the issue, we propose using the main frame ($C4'$, $C1'$, $N1/N9$) in the backbone and four torsion angles $\alpha, \beta, \gamma, \omega$, allowing us to reconstruct the base frame and full-atom coordinates of RNA efficiently. The definition of torsion angles is presented in Figure x. With the base frame, we can enforce the biological constraints, such as base pairing, to optimize the structure module and generate biologically valid structure predictions.

A geometry-aware attention operation, invariant point attention (IPA), is used in modeling the 3D positions. The IPA predicts the rotation and translation matrices for each frame based on the sequence and pair presentation from E2Eformer. In addition, the predicted backbone is refined step by step using a recycling strategy in which the output backbone frame from the previous iteration is provided to the E2Eformer. The recycling process ends when the predicted LDDT (pLDDT) converges, with the pLDDT being one of the outputs generated by the IPA and measuring the quality of the predicted 3D structure. With the predicted main frame and four torsion angles, our structure module can directly generate the full-atom coordinates of an RNA without subsequent simulations.

Details for model training. As there are few structural data available for RNA, we also collected a non-redundant, self-distillation dataset with ground-truth secondary structure from the RNAStralign and bp-RNA-1m databases. In the first training stage, the E2Efold-3D is trained using only PDB data, which is then used to construct a self-distillation dataset by inferring pseudo structural labels. For further improvement, we retrain the model by sampling 25% of the PDB data and 75% of the distillation data. As for the optimizer, Adam is used with a learning rate of 0.0003 for 300,000 iterations. The polynomial decay scheduler is also applied with 10,000 warmup steps, and the batch size is 16. During training, we also apply dropout with ratio as 0.1 at the corresponding layers of the E2Eformer and structure modules.

The structure prediction loss. The loss function is defined by three levels of structural loss: 1D, 2D, and 3D. We will discuss these levels in details. We utilize a masked language modeling loss L_{mlm} to extract co-evolutionary information from the MSA on a 1D level without adding curated correlation features. In our setting, 5% of the tokens are randomly masked, and a linear projection layer is used to reconstruct the masked tokens.

At the 2D level, a distance loss L_{dis} and a secondary structure loss L_{ss} are designated to supervise the E2Efold-3D to learn the pairwise positional correlations between each residue. In particular, three feed-forward layers are considered for distance prediction to predict the pairwise distance between P , $C4$, and N atoms. Distance is divided into 40 bins, where the first and last bins indicate $< 2 \text{ \AA}$ and $> 38 \text{ \AA}$, respectively, and the distance between $[2 \text{ \AA}, 38 \text{ \AA}]$ is evenly divided into 38 bins. Additionally, the cross-entropy loss is used to determine if the distance predictions belong to the correct bin. For the

secondary structure prediction loss L_{ss} , a feed-forward layer is leveraged on top of pairwise features to predict the secondary structure. The secondary structure C is a $L \times L$ binary matrix, where L denotes the sequence length, $C_{i,j} = 0, 1$ indicates that if the i -th and j -th residue form a base pair.

At the 3D level, the gradients come from the main Frame Aligned Point Error (FAPE) loss, an secondary structure constraint loss and a clash violation loss L_{clash} . The FAPE loss proposed in AlphaFold2 scores a set of predicted atom coordinates under a set of predicted local frames against the corresponding ground truth atom coordinates and ground truth local frames. The loss is invariant under rigid motions. When predicted structure differs from the ground truth by an arbitrary rotation and translation, the loss will stay in constant.

The secondary structure constraint loss L_{ss3d} that we propose is to encode secondary structural information directly into 3D prediction. In order to unify the calculation of different types of base pairing constraint in 3D space, we define four pseudo atoms in the base frame ($C1', N1/N9, C/C4$). The L_{ss3d} aims to constrain the pseudo atoms in two base-paired nucleobases to satisfy base-pairing property (spatial closeness). For two residue m and n , we compute the pairwise distance of the four pseudo atoms: $\mathbb{D}^{m,n} = \{d_{i,j}^{m,n} | i, j \in \{1, 2, 3, 4\}\}$, where m and n denote two RNA residues. i and j are the index of the four atoms. We define L_{ss3d} as follows.

$$L_{ss3d} = \sum_{\substack{m=1 \\ n=1}}^{N_{\text{nbpairs}}} \max \left(\mathbf{d}_{i,j}^{m,n} - \tau - \hat{d}_{i,j}^{m,n}, 0 \right), \quad (1)$$

where m, n are the index of two residues that form base pair. $i, j \in \{1, 2, 3, 4\}$ denote the index of four pseudo atoms. $\hat{d}_{i,j}^{m,n}$ is the distance of two pseudo atoms i and j in the predicted structure. $\mathbf{d}_{i,j}^{m,n}$ is the corresponding standard pairwise distance. N_{nbpairs} is the number of all base pair residues in this structure. τ is a tolerance distance threshold. The L_{ss3d} penalizes too far away pairwise atom distance in the nucleobases when two residues form a base pair. The calculation of the standard pairwise distance $\mathbf{d}_{i,j}^{m,n}$ is divided into two scenarios: 1) when the training sample comes from PDB data with 3D native structure, the $\mathbf{d}_{i,j}^{m,n}$ comes directly from the structure; 2) when the training sample comes from self-distilled data, then $\mathbf{d}_{i,j}^{m,n}$ are the statistics values from all PDB structures of the corresponding type of base pair. This can prevent us from overfitting to the pseudo labels, and make full use of secondary structure information.

The L_{clash} expects the model to learn the avoidance of atom clashes by penalizing too short distance between atoms according to their literature Van der Waals radii.

In addition, we use a loss: L_{plDDT} to learn an IDDT evaluator that scores the predicted 3D RNA models as an indicator for global recycling, as introduced above. The L_{plDDT} aims to train a IDDT evaluator that predicts the IDDT of the predicted 3D model against the ground truth structure. The IDDT value is discretized into 50 bins with an interval of 0.02. Once a predicted 3D model is generated, we compute its IDDT against the ground truth structure as the ground truth pIDDT label and the IDDT evaluator produces the predicted pLDDT bin. A cross-entropy loss is employed as L_{plDDT} to calculate if the predicted IDDT falls in the ground truth bin.

The overall loss function is:

$$L = L_{mlm} + 0.3 * L_{dis} + 0.1 * L_{ss} + 0.03 * L_{clash} + 2 * L_{FAPE} + 0.1 * L_{ss3d} + 0.01 * L_{plDDT}. \quad (2)$$

Structure relaxation by AMBER force field. As a preventative measure to resolve any remaining structural clashes and violations, we relaxed our model predictions through a restrained energy minimization procedure. Specifically, we minimize the AMBER force field with harmonic restraints, which allows the system to remain close to its input structure. The post-prediction relaxation also enforces phosphodiester bond geometry precisely. As measured by RMSD and TM-score, empirical evidence

indicates that this final relaxation does not increase the accuracy of the model, but does eliminate distracting stereochemical violations without compromising accuracy.

Implementation details and running time. In terms of the hardware, we used a GPU cluster with a total of 768 GB of memory and eight NVIDIA A100 GPU cards equipped with 80 GB of memory each. The CPU in the cluster is Intel(R) Xeon(R) Gold 6230 CPU @ 2.10GHz with 64 core. E2Efold-3D is trained for 1600 epochs with 300,000 iterations, which takes the cluster approximately one week to complete. However, once the model is trained, the inference process is extremely fast. In the event of a single A100 GPU card, we can predict one structure in 0.14 seconds. In terms of benchmarking FARFAR2, since it is required to generate a large number of structures, it consumes considerable computational time and resources. We perform a Slurm job on the cluster with a single CPU core and 8GB memory and report the running time in Table 4.

References

- [1] Liu, D., Thélot, F. A., Piccirilli, J. A., Liao, M. & Yin, P. Sub-3-Å cryo-em structure of rna enabled by engineered homomeric self-assembly. *Nature Methods* **19**, 576–585 (2022).
- [2] Warner, K. D., Hajdin, C. E. & Weeks, K. M. Principles for targeting rna with drug-like small molecules. *Nature reviews Drug discovery* **17**, 547–558 (2018).
- [3] Kulkarni, J. A. *et al.* The current landscape of nucleic acid therapeutics. *Nature Nanotechnology* **16**, 630–643 (2021).
- [4] Zhao, E. M. *et al.* Rna-responsive elements for eukaryotic translational control. *Nature Biotechnology* **40**, 539–545 (2022).
- [5] Sheridan, C. First small-molecule drug targeting rna gains momentum. *Nature Biotechnology* **39**, 6–9 (2021).
- [6] Xu, B. *et al.* Recent advances in RNA structure. *Science China. Life Sciences* 1–40 (2022).
- [7] Rother, M., Rother, K., Puton, T. & Bujnicki, J. M. Moderna: a tool for comparative modeling of rna 3d structure. *Nucleic acids research* **39**, 4007–4022 (2011).
- [8] Flores, S. C., Wan, Y., Russell, R. & Altman, R. B. Predicting rna structure by multiple template homology modeling. In *Biocomputing 2010*, 216–227 (World Scientific, 2010).
- [9] Watkins, A. M., Rangan, R. & Das, R. Farfar2: improved de novo rosetta prediction of complex global rna folds. *Structure* **28**, 963–976 (2020).
- [10] Wang, J., Wang, J., Huang, Y. & Xiao, Y. 3drna v2.0: An updated web server for rna 3d structure prediction. *International Journal of Molecular Sciences* **20**, 4116 (2019).
- [11] Boniecki, M. J. *et al.* Simrna: a coarse-grained method for rna folding simulations and 3d structure prediction. *Nucleic acids research* **44**, e63–e63 (2016).
- [12] Townshend, R. J. *et al.* Geometric deep learning of rna structure. *Science* **373**, 1047–1051 (2021).
- [13] Jumper, J. *et al.* Highly accurate protein structure prediction with alphafold. *Nature* **596**, 583–589 (2021).
- [14] Chen, X., Li, Y., Umarov, R., Gao, X. & Song, L. Rna secondary structure prediction by learning unrolled algorithms. *arXiv preprint arXiv:2002.05810* (2020).

- [15] Chen, J. *et al.* Interpretable rna foundation model from unannotated data for highly accurate rna structure and function predictions. *arXiv preprint arXiv:2204.00300* (2022).
- [16] Watkins, A. M., Rangan, R. & Das, R. Farfar2: Improved de novo rosetta prediction of complex global rna folds. *Structure* (2020).
- [17] Meyer, M. *et al.* Speciation of a group i intron into a lariat capping ribozyme. *Proceedings of the National Academy of Sciences* **111**, 7659 – 7664 (2014).
- [18] Hoffmann, B. *et al.* Nmr structure of the active conformation of the varkud satellite ribozyme cleavage site. *Proceedings of the National Academy of Sciences* **100**, 7003–7008 (2003). URL <https://www.pnas.org/doi/abs/10.1073/pnas.0832440100>. <https://www.pnas.org/doi/pdf/10.1073/pnas.0832440100>.
- [19] Akiyama, B. M. *et al.* Zika virus produces noncoding rnas using a multi-pseudoknot structure that confounds a cellular exonuclease. *Science* **354**, 1148–1152 (2016). URL <https://www.science.org/doi/abs/10.1126/science.aah3963>. <https://www.science.org/doi/pdf/10.1126/science.aah3963>.
- [20] Mosalaganti, S. *et al.* Ai-based structure prediction empowers integrative structural analysis of human nuclear pores. *Science* **376**, eabm9506 (2022).
- [21] Kalvari, I. *et al.* Rfam 14: expanded coverage of metagenomic, viral and microrna families. *Nucleic Acids Research* **49**, D192 – D200 (2021).
- [22] Sweeney, B. A. *et al.* Rnacentral 2021: secondary structure integration, improved sequence search and new member databases. *Nucleic Acids Research* **49**, D212 – D220 (2021).
- [23] Jumper, J. M. *et al.* Highly accurate protein structure prediction with alphafold. *Nature* **596**, 583 – 589 (2021).